Cytoskeletal actin networks in motile cells are critically self-organized systems synchronized by mechanical interactions

Luca Cardamone, Alessandro Laio[1], Vincent Torre, Rajesh Shahapure[2], and Antonio DeSimone

SISSA, Via Bonomea 265, 34136 Trieste, Italy

Edited by David A. Weitz, Harvard University, Cambridge, MA, and approved July 14, 2011 (received for review January 17, 2011)

Growing networks of actin fibers are able to organize into compact, stiff two-dimensional structures inside lamellipodia of crawling cells. We put forward the hypothesis that the growing actin network is a critically self-organized system, in which long-range mechanical stresses arising from the interaction with the plasma membrane provide the selective pressure leading to organization. We show that a simple model based only on this principle reproduces the stochastic nature of lamellipodia protrusion (growth periods alternating with fast retractions) and several of the features observed in experiments: a growth velocity initially insensitive to the external force; the capability of the network to organize its orientation; a load-history-dependent growth velocity. Our model predicts that the spectrum of the time series of the height of a growing lamellipodium decays with the inverse of the frequency. This behavior is a well-known signature of self-organized criticality and is confirmed by unique optical tweezer measurements performed in vivo on neuronal growth cones.

Actin networks are remarkable biological materials essential for the structural stability of eukariotic cells and for many of their vital functions, including motility (1, 2). They are formed by oriented and branched actin fibers (3) and are able to produce compact and relatively stiff two-dimensional structures such as lamellipodia. Within the lamellipodium of a crawling cell, actin networks are capable of organizing over length scales of several micrometers. Moreover, they are able to grow at an approximately constant velocity, independently of the strength of the external force that opposes their growth (4, 5).

The mechanisms underlying this process have been the object of intense theoretical investigation. The reliability of a model is normally judged from its capability of predicting an almost constant force–velocity (Fv) relationship up to a stall force. In autocatalytic nucleation models (6), when the force increases, the actin network—due to the activity of controlling proteins—originates new branches, so that the velocity v remains constant for increasing values of F, while the density increases accordingly. Other models are based on the idea of Brownian ratchets (7–9): thanks to thermal fluctuations of the membrane, actin filament tips in contact with the membrane become accessible to free actin monomers (and hence to growth by polymerization). These models have been used to explain experimental observations on *Listeria monocytogenes* propulsion (10). The dendritic-nucleation/array-treadmilling model (11) can reproduce the observed geometric structure of actin meshworks near the leading edge of a lamellipodium (12). A symmetric orientation of the actin filaments with respect to the force direction is predicted, provided that branching and capping protection take place only close to the membrane.

The importance of regulatory proteins has been convincingly established in experiments (13–19), and most of the available models focus on biochemical regulation, although mechanical interactions are also known to play an important role (20–30). In refs. 25–28, pulsatile motion of beads propelled by growing actin networks has been observed in models where phases of accumulation of mechanical stresses in the actin filaments alternate with sudden accelerations due to rupture events in the network. These approaches are able to reproduce results from bead and rod motility assays aimed at replicating Listeria motility (24–29). It is suggested in ref. 22 that the mechanical forces arising from actin filament growth against a membrane may provide the basic mechanism for persistent and coordinated cell movement and that, at least in keratocytes, regulatory elements such as signaling molecules may be dispensable or redundant. However, a quantitative assessment of the role of forces in orchestrating organized growth inside protruding lamellipodia is still missing.

Recent advances in experimental techniques have provided detailed information on the dynamics of actin networks (4, 5, 31), both in vivo and in vitro. Very accurate optical tweezer in vivo measurements of the position of a lamellipodium have demonstrated that the leading edge advances with a characteristic "stochastic swing" behavior, in which growth periods alternate with retractions (4). This behavior is observed also when the force exerted by the bead is small, but oscillations increase in size and frequency when the force becomes large. Using the same technique, it was shown that the force necessary to stop completely the growth of the network is of the same order of magnitude of the one exerted by the plasma membrane (4). Thus, also in normal conditions (in the absence of the bead) the propulsive force is almost counterbalanced by the relatively strong tension exerted by the membrane. In this scenario, the retraction periods can be interpreted as due to the pressure exerted by the membrane. Periods of growth alternate with "avalanches" in which the network collapses, at least locally. Why has nature chosen to design the combined system formed by the network and the membrane in this special condition of marginal stability? One may argue that it is not by chance. In fact, the actin network has to produce structures that protrude for several micrometers, and these structures have to be compact and without overhangs in order to be effective for pushing. Avalanches driven by forces arising from the contact with the membrane could be the mechanism that enforces the optimal organization at the micrometer scale.

In order to elaborate on this idea on a quantitative basis, we designed a simple model of lamellipodia growth based only on mechanical ingredients. In the model (see Fig. 1 and *Methods*), the actin network forms by a stochastic process, in which at every "time step" an actin "monomer" is added at the tip (barbed end) of a random filament, forming a time-evolving truss structure. At the

Author contributions: A.L. and A.D. designed research; L.C., A.L., R.S., and A.D. performed research; V.T. directed experimental work; L.C., A.L., and A.D. analyzed data; and L.C., A.L., V.T., and A.D. wrote the paper.

The authors declare no conflict of interest.

This article is a PNAS Direct Submission.

[1]To whom correspondence should be addressed. E-mail: laio@sissa.it.

[2]Present address: Leiden Institute of Chemistry, Gorlaeus Laboratories, Laboratory of Molecular Genetics and Cell Observatory, Leiden University, Leiden, The Netherlands.

This article contains supporting information online at www.pnas.org/lookup/suppl/doi:10.1073/pnas.1100549108/-/DCSupplemental.

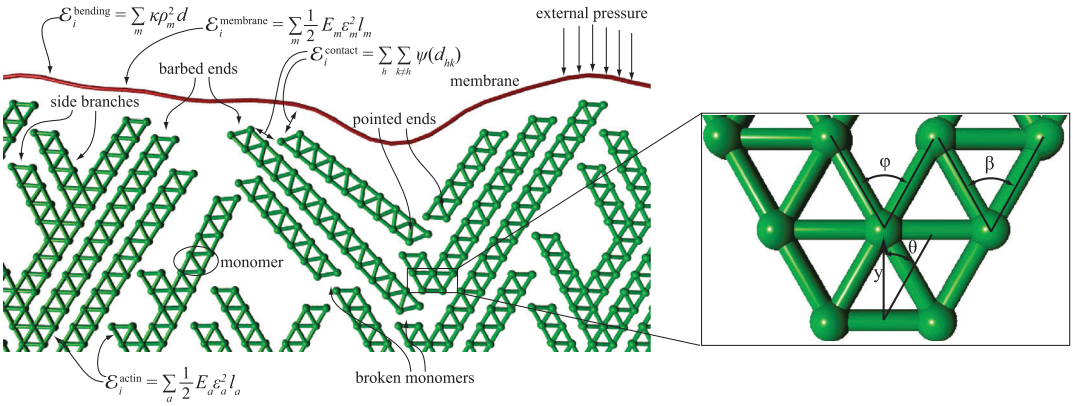

Fig. 1. The model. We consider a two-dimensional network of actin filaments growing against a membrane subject to an external force F directed along the protrusion direction y and opposing the lamellipodium growth. Actin monomers are modeled, as in a truss structure, by two nodes and four connections (edges, the green lines in the figure). Lengths are measured in units of the filament thickness d and forces in units of the filament rupture force F_r. The force F is distributed on a representative cell of width $L_{\text{cell}} = 32\ d$. Periodic boundary conditions are assumed in order to reduce edge effects. At the beginning of the simulation, 12 monomers are created at $y \sim 0$ at an angle θ with the y axis. These seeds are kept fixed throughout the simulation. Time is measured in units of growth steps, in each of which a monomer is added at the tip (barbed end) of a randomly chosen filament. One branching event occurs at a random site along the filaments at every growth step with a probability $P_b = 0.3$. The branching angle φ is fixed at 60° [close to the measured value of 70° (6, 11, 12)]. The contact among different filaments and between filaments and the membrane is modeled by a short-range repulsive potential active for a distance $<d$. In view of the truss geometry, filaments fail if the absolute value of the force in one of the edges exceeds a critical value $f_c = F_r/2$, in which case the overcritical monomer is cleaved. Cleaved filaments, which have an exposed pointed end, depolymerize with a speed of 10 monomers per growth step. We assume the filaments to be linearly elastic up to failure, with a persistence length $\xi = 1{,}000\ d$. This corresponds to approximately 10 μm (35). Reduction to a two-dimensional model is obtained by assuming that a growing planar network deforms a slice of thickness d in the direction orthogonal to the plane of the lamellipodium. The resulting one-dimensional elastic membrane has stretching stiffness of the order of F_r (37) and bending stiffness $\kappa = 0.1 F_r d^2$, which results in a persistence length λd with $\lambda \sim 8 \ll 10^3$ (4, 12). The influence of the parameters on the predictions of the model is discussed in detail in *SI Text*.

beginning of the simulation, "seed" monomers are created at the bottom of the simulation box and kept fixed throughout the computation. Filaments repel each other at a short distance and, with a given probability, branch at a random point. Filaments are allowed to grow and branch if the event does not lead to overlaps with preexisting neighboring filaments or with the membrane (steric hindrance). The network is kept under compressive stress by a flexible membrane, directly interacting with the leading edge of the network. We assume that the polymerization rate is force independent.

The model scale is defined by two independent quantities, the filament diameter d and the filament breaking force F_r. All the other parameters can be expressed in terms of these units as indicated in the caption of Fig. 1. We assumed $d = 7$ nm (19, 32), whereas the critical force for the filament is assumed in the range $F_r = 100$–200 pN (33, 34). The persistence length ξ for the filaments is assumed in the range $\xi = 1$–$2 \times 10^3\ d$ corresponding to about 7–15 μm, which is in agreement with data in refs. 35, 36) (see *SI Text* for further discussion on the choice of parameters). We further assume that a filament pushing against the membrane deforms a slice of a thickness comparable to the filament diameter d. This assumption allows us to estimate the stiffness parameters for our two-dimensional model from experimental measurements of membrane elastic properties. A stretching stiffness approximately $2F_r$ used in the model corresponds to an in-plane stretching modulus of the order of 100 pN/nm, in agreement with ref. 37. The bending modulus $\kappa = 0.1 F_r d^2$ corresponds to a bending stiffness of approximately 20 $K_B T$, consistent with refs. 4 and 12.

After each growth event, we compute the local stress on each of the actin monomers by minimizing the total potential energy of the network using a computer program (38). If the stress in a monomer becomes higher than a critical threshold, the monomer breaks and the filament depolymerizes from its pointed end. A similar scheme of filament crushing and disassembly at the trailing edge has been recently proposed in ref. 23 as a key mechanism for shape regulation in fish keratocytes.

We avoided on purpose including in the model the effect of a regulating network based on biochemistry (e.g., we do not model explicitly the selective capping of filaments far from the membrane). This regulating network is present in living cells but, as we will see, its presence is not essential for explaining many key features of the available experimental evidence. For fish keratocytes, this has already been suggested in ref. 22. One may then speculate that biochemical regulation could have appeared later in evolution in order to *optimize* the performance of the system, building on a simpler prototype based only on mechanical regulation. Also other effects (cross-links between actin fibers, membrane-cytoskeleton adhesion, etc.) are neglected in our model because they are not strictly necessary for stress transmission in the compressive regime arising inside the network when it grows against the membrane, or when the lamellipodium pushes against an obstacle.

Results

The results reported here refer to the benchmark values of the model parameters reported in Table S1. A typical outcome of our simulations is shown in Fig. 2, where we plot the height of the lamellipodium as a function of time. It is evident that growth proceeds alternating protrusions and fast retractions. Cleavage events are marked by crosses in Fig. 2. This behavior closely resembles the experimental traces at high time resolution (4). The emergence of a strongly organized structure, such as the one depicted in Fig. 2 *Inset A*, *Top Left* that leads to a protrusion of almost 50 times the filament thickness d, is obtained after many attempts, in which the system collapses almost completely at much smaller heights (see Movie S1). Less catastrophic retractions are observed also when the system is finally able to grow, after $t = 1{,}800$. These retractions are indeed crucial to achieve a sufficient structural stability, as in these events "unfit" filaments are cleaved and eliminated. In other words, if the filaments would not break, the system would not be able to produce a compact and organized structure capable of sustaining a significant external pressure. This scenario, in which mutation is guaranteed by random growth and branching, while selection is achieved through failure of the overstressed filaments, is strongly reminiscent of the evolutionary model in ref. 39. Due to the pressure exerted by the membrane, the actin network organizes itself into a close packed structure, in which each branch is sustained by several other branches (Fig. 2 *Inset A*, *Top Left*).

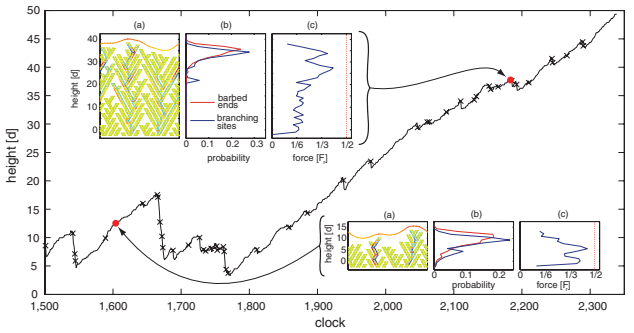

Fig. 2. Growth, stress diffusion, and localization of the active area near the membrane. Height as function of growth clock for a benchmark simulation of a pushing event against an applied force F of $0.5F_r$. Crosses correspond to failure events. *Insets A* report the network configuration at two different times. Monomers under compressive (respectively, tensile) stress are colored in blue (respectively, red). *Insets B* show the height distribution of the sites where new monomers can be added (barbed ends) and where new branches can appear (branching sites). Distributions are computed over several independent configurations of height 38 $d \sim 270$ nm (*Top Left*) and 13 $d \sim 90$ nm (*Bottom Right*). *Insets C* report, for the same configurations as *A*, the magnitude of the maximum force in the monomers as a function of height.

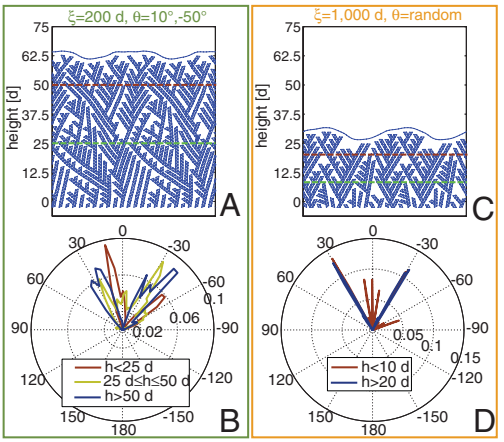

Fig. 3. Network reorientation. (*A*) Representative configuration of a simulation of a pushing event against an applied force $1/2F_r$ with $\xi = 200\ d$ and seeds oriented at $\theta = 10°, -50°$. This small persistence length allows an easy angular reorganization of the filaments. (*B*) Distribution of filament orientation for different height ranges for cases like the one in *A*. (*C*) Representative configuration of a simulation of a pushing event against an applied force $1/2F_r$ with $\xi = 1{,}000\ d$ and random orientation of the initial seeds. (*C*) Distribution of filament orientation for different height ranges for cases like the one in *C*.

Just as in autocatalytic (6) and dendritic-nucleation/array-treadmilling models (11), during organized growth all the relevant events (polymerization, branching, and cleavage) happen in a relatively thin layer close to the membrane, while the rest of the network reaches a steady state. This is demonstrated in Fig. 2 *Insets B*, where we plot the probability of observing a branching and a polymerization event as a function of height (averages are taken over several independent simulations). In contrast with the other models (6, 11), these peaked distributions are not imposed a priori but stem only from the mechanical properties of the system: Monomers buried deeply into the network, and far away from the membrane, are mechanically shielded (low stress levels and no growth or branching because of lateral support and steric hindrance). However, it is obvious that selective localization of suitable proteins and enzymes, which catalyze branching and growth in the proximity of the membrane (6, 11, 40), can greatly enhance the efficiency of the system (e.g., by decreasing the waiting time for the formation of configurations that are fit for pushing).

Another important feature of our model is that during organized growth the stress is uniformly distributed throughout the network. In Fig. 2 *Insets A* the monomers are colored according to the local stress, with red indicating traction and blue compression. Clearly, the stress is modest and uniformly distributed at all heights. Fig. 2 *Insets C* show the maximum absolute value of the force as a function of height, highlighting that it is more evenly distributed and lower in average in the case of an organized geometry (*Top Left*) compared to the cases of a nonorganized one (*Bottom Right*). Moreover, it is clear how the maximum force near the bottom of the simulation box is high for nonorganized networks, whereas it is close to zero for organized structures. This is an important feature, because ruptures of the network near the bottom cause global, catastrophic avalanches.

Filament Orientation. Because of the pressure exerted by the membrane, the network is capable of reaching a global geometric organization by automatically aligning the bisectrix of the branching angle with the external force. In Fig. 3*A* we show a typical configuration reached starting from an initial state in which the filaments are "misoriented" (i.e., $\theta = 10°, -50°$) but very flexible ($\xi = 200\ d$). Indeed, as shown in Fig. 3*B*, the orientation of monomers below 25 d is strongly affected by the initial orientation of the seeds that, in the example in Fig. 3*B*, are generated with a probability strongly peaked around $-10°$ and $50°$ (red curve). The distribution above 50 d, instead, shows only two significant peaks around $\pm 30°$ (blue curve). The symmetric pattern we obtain is in agreement with experiments (39) and reproduces, relying only on mechanics, the results obtained in ref. 11. A similar numerical experiment has been conduced for randomly oriented, regularly stiff filaments ($\xi = 1{,}000\ d$). The configuration reported in Fig. 3*C* shows how only the filaments with symmetric orientation with respect to the force direction are selected by the growth-cleavage-depolymerization process. The selection is extraordinarily clear in the sharp orientation distribution reported in Fig. 3*D* and takes place on a very short length scale (about 20 d). Thus the mechanics of the system suggests two distinct mechanisms to explain the observed symmetry of filaments orientation: rotation due to filament flexibility (over a long range) and selection due to cleavage–depolymerization of misoriented filaments (over a shorter range).

Velocity. The model also predicts that fit networks grow with an almost constant force–velocity relationship. In Fig. 4*A* we report the time histories of the network height for different values of the forces. It is evident that, when organized growth takes place, the height traces are roughly parallel to each other independent of the level of the force. However, retraction events are more frequent and severe for higher values of the force. In Fig. 4*B* we report the distribution of the velocity of the advancing front. Increasing the force broadens the velocity distribution, but affects much less the position of the maximum. At $F > 0.6F_r$, the center of the distribution collapses to zero, and the observation of positive velocities becomes unlikely. The value of the most likely velocity is plotted against force intensity in Fig. 4*C*. Such a plot shows a strong nonlinear dependence of the velocity on the force, with an almost flat behavior at low forces and a stalling force of about $0.6F_r$. This behavior closely resembles the experimental Fv curves, measured by atomic force microscopy (AFM) (5, 31) and optical tweezers (4). The curve is well fitted by the relation $v = v_0(1 - F/F_{\text{stall}})^4$, where F_{stall} is the stalling force and v_0 is the velocity under zero force, similar to the one proposed in ref. 22. In our model, the approximately constant Fv behavior is a consequence of the capability of the network of adjusting to variable force levels by reorganizing its geometric structure. At the same time, the network becomes slightly more dense as reported in Fig. 4*C*, *Inset*, in agreement with numerical findings in ref. 6.

Given the geometry that we consider in this work (see Fig. 1), a stalling force of $0.6F_r$ corresponds to approximately $0.05F_r$ acting on each filament in contact with the membrane. With $F_r \sim$

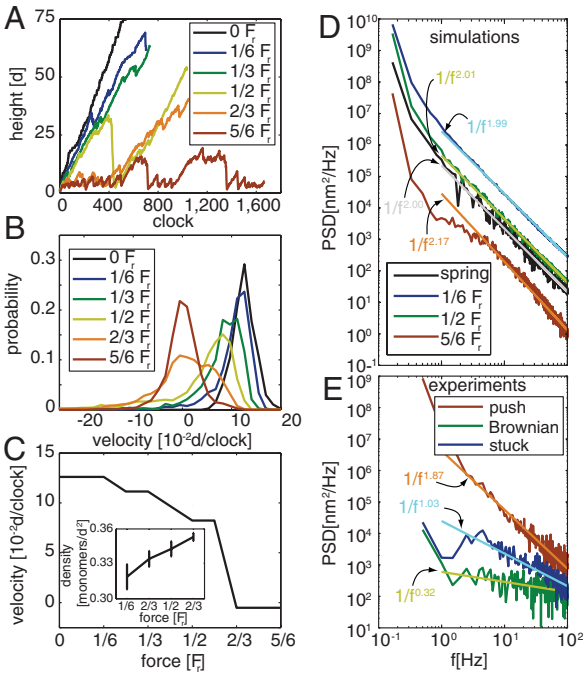

Fig. 4. Growth velocities, hysteresis, stochastic swing, and self-organized criticality. (*A*) Representative traces for simulated pushing experiments at different force levels. (*B*) Probability distribution of the velocity at different force levels. The velocity is estimated from the slope of the linear regression over a rolling window of 100 growth steps. Histograms are computed taking the average over at least 10 independent simulations like those depicted in *A*. (*C*) Most likely velocity as a function of the force. (*Inset*) Reports the average density of the network as a function of the applied force. Error bars represent the standard deviation of this quantity. (*D*) PSDs and their best linear fit for simulated traces at different values of force and growth against linear spring. (*E*) PSDs and their best linear fit for the traces measured in optical tweezer experiments on neuronal growth cones during Brownian oscillation of the bead, for the bead stuck on the coverslip, and pushing action of the lamellipodium. Experimental PSDs are shown up to the cutoff frequency of the trap (100 Hz) as above this frequency the spectrum is strongly modified by the experimental setup (4).

100 pN, we find that, according to our model, the growth of a lamellipodium can be stopped by applying an external force of a few piconewtons per filament in contact with the membrane. As already found elsewhere (4), this force is of the order of magnitude of the restraining force exerted by the membrane: For a lamellipodium slice of thickness d and width $L_{cell} = 32\ d$ this force is of the order of $2\gamma L_{cell}$ where $\gamma = 0.005\ K_B T$ is the membrane surface tension (4, 12). The resulting estimated force per filament is $0.09F_r$ corresponding to 9 pN. This estimate is probably an upper bound, as it assumes that most of the surface tension is sustained by a single layer, as it would happen if the front is rounded (12). In order to be more quantitative on this estimate, one should model the system in three dimensions.

In the simulations, branch junctions are usually assumed to have the same resistance as the filaments. To check the effect of possible preferential breaking at branching sites, we performed simulations doubling the filaments resistance without changing the resistance of the branching points. We obtain very similar results in terms of filament orientations and Fv diagrams, with geometries showing shorter side branches (see *SI Text*). These results suggest that the Fv curve is controlled by the resistance of the weak points in the network.

Hysteresis. Because the network geometry may evolve, the growth velocity at a given force level depends on the load history, as also observed experimentally (31). Indeed, a network that has survived a high force level is extremely fit and can withstand lower forces more easily. In this network, large avalanches will be more unlikely, and the velocity distribution will be shifted toward larger positive values (see *SI Text*). We conclude that the multiplicity of velocities under the same applied force, and the resulting hysteretic Fv response are natural consequences of the morphological changes from one stable network structure to another, occurring when a lamellipodium grows against a time-dependent applied force. A similar idea has been put forward in ref. 41, where hysteresis arises from transitions between two fixed metastable geometric configurations. In our approach hysteresis is triggered by the same selection mechanism that leads to organized growth.

Self-Organized Criticality. The most peculiar feature of our model is that mechanical stress is the key factor that leads to geometric organization. Systems evolving in conditions of spatial or temporal self-organization as a consequence of an external stress or pressure are rather common in nature. A clear signature of this scenario is the onset of a power-law distribution in spatial or time correlations (42). Not surprisingly, our model shows very clearly this signature, as it is basically equivalent to a two-dimensional sand pile, with the membrane tension playing the role of gravity. As shown in Fig 4*D*, the power spectral density (PSD) of the front height decays as $1/f^{\alpha}$, where f is the frequency, and the exponent α is approximately equal to two regardless of the intensity of the force. The same signature is observed for the simulated growth against a linear spring. One immediately wonders if also experimental traces show these features.

In order to answer this question, we performed accurate measurements of the position of the front of a lamellipodium by an optical tweezer. Neurons from dorsal root ganglia (DRG) of P10-P12 rats were isolated and plated on poly-L-lysine-coated glass coverslips, positioned on the stage of an inverted microscope used for imaging and for force measurements (4). After 1 or 2 d of incubation, lamellipodia emerged and silica beads were trapped with an infrared optical tweezer in front of the lamellipodia. The bead position was measured at 10-kHz temporal resolution with a quadrant position detector using back focal plane interferometry (43). As the lamellipodium grows, the bead is pushed away from the center of the trap. This allows for a simultaneous measurement of the force and of the velocity of the lamellipodium front (4). In a typical experiment the bead remains detached from the lamellipodium, and its position fluctuates significantly due to Brownian motion. In these conditions, the PSD of the position of the front is flat up to the cutoff frequency of the trap (10^2 Hz in our case). In rare cases, adhesion forces caused the bead to seal onto the lamellipodium. In these conditions, the amplitude of fluctuations of the bead decreases significantly, and it is possible to measure the position of the lamellipodium front with a very good temporal resolution. In Fig. 4*E* we report the PSD of bead displacements during such an adhesion phase. Remarkably, it decays as $1/f^2$, in a manner that closely resembles the numerical results of Fig. 4*D*. For comparison, in Fig. 4*E* we also show the spectrum in a noncontact phase and in a control experiment in which the bead is stuck on the poly-L-lysine-coated coverslip. The different PSD decay in this latter case proves that the signature of the lamellipodium growth is not due to environmental noise.

Discussion

In summary, we have shown that a model based on the mechanical interaction between a growing stiff network of collaborating filaments and a flexible membrane is capable of explaining many seemingly unrelated features of the observed behavior of growing lamellipodia: a growth velocity initially insensitive to the external force up to a stalling value; the capability of the network to organize its orientation with respect to the applied force; a load-history-dependent growth velocity; the concentration of the branching/capping protection zone near the membrane. The model predicts that the range of external forces for which growth can

take place is in the 10^{-2}–10^{-1} pN/nm range. In normal conditions, this is exerted by the membrane, which is then responsible for exerting the "selective pressure" on the network. The range of forces predicted by our model is just marginally larger than $2 * 0.02$ pN/nm, the restraining force per unit length exerted by surface tension on a growing lamellipodium (12), and of the same order of magnitude of $2 * 0.1$ pN/nm, the force exerted by the membrane according to the estimate for a crawling keratocyte (22).

In our model, we assumed for simplicity that the polymerization rate is not explicitly force-dependent. However, the filaments on which a monomer is added are not chosen at random, as growth events that would lead to overlaps with preexisting filaments or with the membrane are not allowed (see *Methods*). As a consequence, the axial forces on filaments selected for growth are always rather low. In fact, we computed the probability distribution of the axial forces acting on the filaments on which a new monomer is added during 12 statistically independent histories of growth against different external forces (see *SI Text*). Even when the network grows against the comparatively large external force of $0.5F_r$, the axial force on growing filaments is zero in 40% of the cases and is larger than $1/6F_r$ only in about 1% of the cases. Introducing a genuine force-dependent rate of polymerization would certainly be an interesting theme for further studies. However, modeling exactly this effect may require precise experimental information on the growth dynamics of isolated filaments, extending the results in ref. 44.

Our model provides an explanation for the stochastic nature of the motion of the leading edge observed in experiments, where growth periods alternate with fast retractions. In fact, we claim that these retractions are *essential* in order to make our growth mechanism robust. This has an important and nontrivial consequence on the statistics of these retractions, whose amplitude and frequency are *predicted* to obey a power-law distribution, as in critically self-organized systems. This prediction is confirmed by our experiments on neuronal growth cones, showing that the PSD of the time series of the height of a growing lamellipodium decays with the square inverse of the frequency. It is well known that in conditions of self-organized criticality power-law distributions should emerge also in other observables, such as the amplitude of the retractions or the correlation between the height of the front in two different locations. The presence of these power laws is a direct consequence of the model we propose here and offers a direct manner of falsifying or confirming its validity when even more accurate experimental data will become available.

Retraction events may play an important role in all processes where motility rests on the buildup of compressive stresses in actin filaments (structures that, without some form of organization and coordination, would be ill-equipped to sustain compressive and bending stresses). These are ubiquitous in actin cell motility, including systems exhibiting pulsatile motion such as Listeria and motility assays (25–28). In bead motility assays, for example, pauses (during which stresses accumulate in the growing network) alternate with sudden accelerations of the whole bead (due to the breakup of transient attachments and fracture of shells of filaments encapsulating the bead). Although these velocity fluctuations involve macroscopic spatial and temporal scales, the ones occurring in the active layer forming at the leading edge of a protruding lamellipodium, between the plasma membrane and the previously grown, immobilized network, take place at microscopic scales. In our scheme, these fluctuations are the means to achieve network geometries that are effective for pushing the lamellipodium forward and generate sustained motility. Retractions and jerky motion at microscopic scales are compatible with smooth motion without significant oscillations at macroscopic scales. Thus, we believe that our scheme of mechanical self-organization through accumulation of mechanical stresses and avalanches of breaking events may be relevant for other actin-based motile systems, besides the neural growth cones studied in this paper.

Model

In the model developed in this work, the actin network forms by a stochastic process driven by an energy function defining the interaction between the filaments and between the filaments and the membrane. At the ith growth step, the energy of the system $\mathscr{E}_i$ is a function of the position of the nodes $\{u\}_i$. The equilibrium configuration of the nodes $\{u^{\mathrm{eq}}\}_i$ is obtained by minimizing $\mathscr{E}_i$ numerically, via a conjugate gradient method implemented in the Surface Evolver package (38)

$$\{u^{\mathrm{eq}}\}_i = \mathrm{argmin}_{\{u\}_i}\, \mathscr{E}_i(\{u\}_i). \qquad [1]$$

We assume the actin filaments to be linearly elastic up to failure and the membrane to have a linear elastic in-plane behavior. The filaments are represented by a truss structure, namely, a bead and spring model where the spring constant is the stretching stiffness E_a of the edges. The bending stiffness of the filaments is related to the persistence length ξ by the classical statistical mechanics result $\kappa_a = 2\xi K_{\mathrm{B}}T$, where κ_a is the equivalent bending stiffness of the truss structure modeling the actin filaments. In turn, from simple geometry and statics, the bending stiffness of the filament κ_a can be related to the stiffness of the trusses, namely $\kappa_a = 2E_a(a\tan\beta/4)^2$, where $\beta = 60°$ is the characteristic angle of the truss edges (see Fig. 1). Equating the two expressions for κ_a, we obtain

$$E_a = \frac{16\xi K_b T}{a^2\tan^2\beta}, \qquad [2]$$

and the elastic energy for the whole actin network is

$$\mathscr{E}_i^{\mathrm{actin}} = \sum_a \frac{1}{2}E_a\epsilon_a^2 l_a, \qquad [3]$$

where ϵ_a is the extensional strain of the actin edge a, and l_a is its undeformed length. A similar energy is considered for the membrane

$$\mathscr{E}_i^{\mathrm{membrane}} = \sum_m \frac{1}{2}E_m\epsilon_m^2 l_m. \qquad [4]$$

The membrane is assumed to have also a bending stiffness κ that penalizes its curvature ρ. The bending energy of a slice of thickness d is of the form

$$\mathscr{E}_i^{\mathrm{bending}} = \sum_m \kappa\rho_m^2 d, \qquad [5]$$

where ρ_m is the curvature computed distributing the angle at the node m of the discretized membrane over a length d (equal to the membrane discretization length). The bending stiffness of the membrane corresponds to a persistence length $\xi_m = \kappa/2\ K_{\mathrm{B}}T \sim 8\ d$ for the parameter values used in the model.

Contact among different filaments is modeled by introducing a short-range repulsion energy ψ between the nodes. Given a pair of nodes h and k, ψ is a function of the distance d_{hk} between the two nodes, and the contribution to the overall energy of the system is given by

$$\mathscr{E}_i^{\mathrm{contact}} = \sum_h \sum_{k\neq h} \psi(d_{hk}). \qquad [6]$$

We take for ψ the functional form

$$\psi(d_{hk}) = \begin{cases} c\left[\left(\frac{d_{hk}}{\delta}\right)^{-4} - 2\left(\frac{2d_{hk}}{\delta}\right)^{-2} + 2^{-4}\right] & d_{hk} \le 2\delta \\ 0 & d_{hk} > 2\delta \end{cases}, \qquad [7]$$

where c is a constant. The contact force goes to infinity for vanishing distance and vanishes smoothly when the distance is larger than the threshold length 2δ. Contact between filaments and membrane is modeled in precisely the same way except that, in this case, the contact length parameter 2δ is used. Besides governing force transmission and mechanical collaboration between filaments, detection of contact also allows us to limit uncontrolled growth of the filaments. Indeed, we discard growth events on a filament that would lead to overlap with neighboring filaments. This makes an explicit modeling of capping unnecessary. This approximation should probably be reconsidered if the model is extended to

3D. The larger contact length parameter for filament–membrane interactions leads to a typical separation between filaments and membrane larger than one monomer and mimics the impact of the high flexibility of the membrane (20, 35, 37) on the dynamics of growth: Adding a monomer against the membrane is allowed because membrane ripples, triggered by thermal fluctuations, allow monomers to reach the barbed ends. Instead, growth against other filaments is less likely, as filaments are more rigid and fluctuations are unlikely to create enough room for an extra monomer. We typically consider constant external forces of intensity F pushing down the membrane nodes: $\mathscr{L}_i^{\text{ext}} = -F\sum_h y_h$. We also seek to model the protrusion of a lamellipodium against an elastic spring. In this case the work of the external forces is given by $\mathscr{L}_i^{\text{ext}} = -K\bar{y}\sum_h y_h$, where $\bar{y}$ is the mean height of the membrane and K is a stiffness constant. Summarizing, the energy of the system is

$$\mathscr{E}_i = \mathscr{E}_i^{\text{actin}} + \mathscr{E}_i^{\text{membrane}} + \mathscr{E}_i^{\text{bending}} + \mathscr{E}_i^{\text{contact}} - \mathscr{L}_i^{\text{ext}}. \qquad [8]$$

Experimental Methods

Neuron preparation. Rats (P10-P12) were anesthetized with CO_2 and sacrificed by dislocation in accordance with the Italian Animal Welfare Act. DRGs were incubated with trypsin (0.5 mg/mL, Sigma-Aldrich), collagenase (1 mg/mL, Sigma-Aldrich), and DNase (0.1 mg/mL, Sigma-Aldrich) in 5 mL neurobasal medium (Gibco, Invitrogen) in a shaking bath (37 °C, 35–40 min). DRGs were mechanically dissociated, centrifuged at $300 \times g$, resuspended in culture medium, and plated on poly-L-lysine-coated (0.5 μg/mL, Sigma-Aldrich) coverslips. Cells were incubated for 24 to 48 h followed by the addition of nerve growth factor (50 ng/mL; Alomone) before the measurements.

Optical Tweezer Setup. The optical tweezers setup was built as previously described (43). The dish containing the differentiating neurons and the beads (PSI-1.0NH2, G.Kisker GbR) was placed on the microscope stage, which could be moved by a three-axis piezoelectric nanocube (17 MAX 301, Melles Griot Inc.). The temperature of the dish was kept at 37 °C by a Peltier device. The bead position was determined in the x, y, and z planes with a lateral and axial accuracy of 2 and 5 nm, respectively, which was obtained from the analysis of the interference between forward scattered light from the bead and unscattered light (43, 45). The back focal plane of the condenser was imaged onto a QPD (C5460SPL 6041, Hamamatsu), and the light was converted to differential outputs digitized at 10 kHz and low pass filtered at 5 kHz. Both the lateral and axial trap stiffness, $\mathbf{k}_{xy} = (k_x, k_y)$ and k_z, respectively, as well as the detector sensitivity were calibrated using the power spectrum method (43) with voltage signals filtered and digitized at 5 kHz. In order to reduce and possibly avoid all mechanical perturbations affecting the measurement of $\mathbf{x} = (x,y,z)$, the optical tweezers setup was kept in an isolated and soundproof room, and the scientists performing the experiments controlled all operations remotely from a separate room, in order to reduce perturbations, which could have affected previous investigations.

1. Pollard T, Blanchoin L, Mullins R (2000) Molecular mechanisms controlling actin filament dynamics in nonmuscle cells. *Annu Rev Biophys Biomol Struct* 29:545–576.
2. Pollard T, Borisy G (2003) Cellular motility driven by assembly and disassembly of actin filaments. *Cell* 112:453–465.
3. Schaub S, Meister J, Verkhovsky A (2007) Analysis of actin filament network organization in lamellipodia by comparing experimental and simulated images. *J Cell Sci* 120:1491–1500.
4. Shahapure R, et al. (2010) Force generation in lamellipodia is a probabilistic process with fast growth and retraction events. *Biophys J* 98:979–988.
5. Prass M, Jacobson K, Mogilner A, Radmacher M (2006) Direct measurement of the lamellipodial protrusive force in a migrating cell. *J Cell Biol* 174:767–772.
6. Carlsson AE (2003) Growth velocities of branched actin networks. *Biophys J* 84:2907–2918.
7. Peskin CS, Odell GM, Oster GF (1993) Cellular motions and thermal fluctuations: The Brownian ratchet. *Biophys J* 65:316–324.
8. Mogilner A, Oster G (1996) Cell motility driven by actin polymerization. *Biophys J* 71:3030–3045.
9. Mogilner A, Oster G (2003) Force generation by actin polymerization II: the elastic ratchet and tethered filaments. *Biophys J* 84:1591–1605.
10. Mogilner A (2006) On the edge: Modeling protrusion. *Curr Opin Cell Biol* 18:32–39.
11. Schaus T, Taylor E, Borisy G (2007) Self-organization of actin filament orientation in the dendritic-nucleation/array-treadmilling model. *Proc Natl Acad Sci USA* 104:7086–7091.
12. Atilgan E, Wirtz D, Sun S (2005) Morphology of the lamellipodium and organization of actin filaments at the leading edge of crawling cells. *Biophys J* 89:3589–3602.
13. Machesky L, Atkinson S, Ampe C, Vandekerckhove J, Pollard T (1994) Purification of a cortical complex containing two unconventional actins from Acanthamoeba by affinity chromatography on profilin-agarose. *J Cell Biol* 127:107–115.
14. Mullins R, Heuser J, Pollard T (1998) The interaction of Arp2/3 complex with actin: Nucleation, high affinity pointed end capping, and formation of branching networks of filaments. *Proc Natl Acad Sci USA* 95:6181–6186.
15. Cooper J, Schafer D (2000) Control of actin assembly and disassembly at filament ends. *Curr Opin Cell Biol* 12:97–103.
16. Yang C, et al. (2000) Profilin enhances Cdc42-induced nucleation of actin polymerization. *J Cell Biol* 150:1001–1012.
17. Lu J, Pollard T (2001) Profilin binding to poly-L-proline and actin monomers along with ability to catalyze actin nucleotide exchange is required for viability of fission yeast. *Mol Biol Cell* 12:1161–1184.
18. Watanabe N, Mitchison T (2002) Single-molecule speckle analysis of actin filament turnover in lamellipodia. *Science* 295:1083–1083.
19. Pollard TD, Earnshaw WC (2008) *Cell Biology* (Saunders, New York).
20. Atilgan E, Wirtz D, Sun S (2006) Mechanics and dynamics of actin-driven thin membrane protrusions. *Biophys J* 90:65–76.
21. Kruse K, Joanny JF, Jülicher F, Prost J, Sekimoto K (2005) Generic theory of active polar gels: A paradigm for cytoskeletal dynamics. *Eur Phys J E Soft Matter* 16:5–16.
22. Keren K, et al. (2008) Mechanism of shape determination in motile cells. *Nature* 453:475–480.
23. Mogilner A, Rubinstein B (2010) Actin disassembly 'clock'and membrane tension determine cell shape and turning: A mathematical model. *J Phys Condens Matter* 22:194118.
24. Loisel T, Boujemaa R, Pantaloni D, Carlier M (1999) Reconstitution of actin-based motility of Listeria and Shigella using pure proteins. *Nature* 401:613–616.
25. Alberts J, Odell G (2004) In silico reconstitution of Listeria propulsion exhibits nanosaltation. *PLoS Biol* 2:e412.
26. Van Der Gucht J, Paluch E, Plastino J, Sykes C (2005) Stress release drives symmetry breaking for actin-based movement. *Proc Natl Acad Sci USA* 102:7847–7852.
27. Burroughs N, Marenduzzo D (2007) Nonequilibrium-driven motion in actin networks: Comet tails and moving beads. *Phys Rev Lett* 98:238302.
28. Dayel M, et al. (2009) In silico reconstitution of actin-based symmetry breaking and motility. *PLoS Biol* 7:e1000201.
29. Achard V, et al. (2010) A primer-based mechanism underlies branched actin filament network formation and motility. *Curr Biol* 20:423–428.
30. Sykes C, Plastino J (2010) Cell biology: Actin filaments up against a wall. *Nature* 464:365–366.
31. Parekh S, Chaudhuri O, Theriot J, Fletcher D (2005) Loading history determines the velocity of actin-network growth. *Nat Cell Biol* 7:1219–1223.
32. Alberts B, et al. (2008) *Molecular Biology of the Cell* (Garland Science, New York).
33. Kishino A, Yanagida T (1988) Force measurements by micromanipulation of a single actin filament by glass needles. *Nature* 334:74–76.
34. Tsuda Y, Yasutake H, Ishijima A, Yanagida T (1996) Torsional rigidity of single actin filaments and actin-actin bond breaking force under torsion measured directly by in vitro micromanipulation. *Proc Natl Acad Sci USA* 93:12937–12942.
35. Gittes F, Mickey B, Nettleton J, Howard J (1993) Flexural rigidity of microtubules and actin filaments measured from thermal fluctuations in shape. *J Cell Biol* 120:923–934.
36. Isambert H, et al. (1995) Flexibility of actin filaments derived from thermal fluctuations. Effect of bound nucleotide, phalloidin, and muscle regulatory proteins. *J Biol Chem* 270:11437–11444.
37. Wolfe J, Steponkus P (1983) Mechanical properties of the plasma membrane of isolated plant protoplasts: Mechanism of hyperosmotic and extracellular freezing injury. *Plant Physiol* 71:276–285.
38. Brakke K (2008) *The Surface Evolver*, http://www.susqu.edu/brakke/evolver/evolver.html.
39. Maly I, Borisy G (2001) Self-organization of a propulsive actin network as an evolutionary process. *Proc Natl Acad Sci USA* 98:11324–11329.
40. Fletcher D, Theriot J (2004) An introduction to cell motility for the physical scientist. *Phys Biol* 1:T1–T10.
41. Weichsel J, Schwarz U (2010) Two competing orientation patterns explain experimentally observed anomalies in growing actin networks. *Proc Natl Acad Sci USA* 107:6304–6309.
42. Bak P, Tang C, Wiesenfeld K (1987) Self-organized criticality: An explanation of $1/f$ noise. *Phys Rev Lett* 59:381–384.
43. Neuman K, Block S (2004) Optical trapping. *Rev Sci Instrum* 75:2787–2809.
44. Footer M, Kerssemakers J, Theriot J, Dogterom M (2007) Direct measurement of force generation by actin filament polymerization using an optical trap. *Proc Natl Acad Sci USA* 104:2181–2186.
45. Kress H, Stelzer E, Griffiths G, Rohrbach A (2005) Control of relative radiation pressure in optical traps: Application to phagocytic membrane binding studies. *Phys Rev E Stat Nonlin Soft Matter Phys* 71:061927.

Supporting Information

Cardamone et al. 10.1073/pnas.1100549108

SI Text

Model Parameters. Numerical simulations in the main text have been performed with the parameter values reported in Table S1 (if not specified otherwise) to which we refer as the "benchmark" set of parameters.

The two most critical parameters are the filament breaking force F_r and their persistence length ξ, because they are strongly affected by several factors, such as filament decoration and loading condition. Experimental estimates for the breaking force in tension vary in the range 100–600 pN (1, 2) depending on whether the filament is subject to torsion. In our simulations filaments break in bending and the value of $F_r = 100$ pN used in the benchmark simulations gives a critical bending moment $F_r d/2 = 350$ pN · nm, which is very close to the one estimated from ref. 3 using $K/\rho^* = 306$ pN · nm, where K is the bending stiffness and ρ^* is the critical bending radius. Fig. S1 shows that the Fv curves obtained with $\{F_r = 100$ pN,$\xi = 7$ μm$\}$ and $\{F_r = 200$ pN, $\xi = 15$ μm$\}$ are very similar. The range of variability of ξ is compatible with data in ref. 4 for a different kind of actin-binding proteins.

Movie S1. Movie S1, also downloadable from http://people.sissa.it/~desimone/Movies/ActinMovie.avi, shows the simulation of an actin network growing against a force of $0.5F_r$. (*Top Left*) We plot the distribution of the maximum stress with height. (*Top Right*) This shows the time history of the advancing front; crosses indicate time instants where ruptures take place while the current position is indicated by the moving red dot. (*Lower*) The evolving network configuration is shown; beams are colored according to the stress experienced (red indicates traction and blue compression).

Sensitivity to the Parameters. In order to analyze the sensitivity of our results to changes in the parameters, we performed simulations varying one parameter at a time with respect to the values reported in Table S1. Fig. S2 summarizes the influence of structural parameters on the growth of the lamellipodium. In Fig. S2*a* we report the height distribution for various choices of branching probability, seed orientation, filament stiffness, and membrane stiffness. Reduced branching leads to less organized structures and penalizes lamellipodium growth. Reducing branching probability also leads to shorter protrusions (the height of the lamellipodium remains confined below 25 d). A symmetric distribution of initial seeds leads to a more effective configuration compared with the one with seeds at $\theta = +10°, -50°$, and this confirms the finding in ref. 5 that the filaments are preferentially organized in two symmetric families with respect to the growth direction. Asymmetric configurations rarely lead to lamellipodium growth above 12.5 d, whereas the height distribution is almost flat up to 50 d for symmetric growth. Filament stiffness has a very strong, and somewhat surprising, effect on the lamellipodium growth. Indeed, stiffer filaments lead to less effective protrusion. This phenomenon is explained by the fact that stiffer filaments break before being able to exploit the supporting action of neighbors, whereas softer filaments can bend more before breaking, enhancing the capability of the network to dissipate stress concentrations by lateral diffusion. The effect of filament stiffening ($\xi = 2{,}000$ d) is the most dramatic one and constrains the lamellipodium to fast oscillations that rarely go above 10 d in height. With softer filaments ($\xi = 200$ d) the lamellipodium grows easily above 50 d. The histograms of mesoscopic velocity distributions in Fig. S2*b* confirm that lower branching probability, nonsymmetric networks, and stiffer filaments all lead to less effective pushing action. The black curves in Fig. S2 depict the effect of a tenfold increase in membrane bending stiffness. The lamellipodium growth is slower with respect to the benchmark case and this can be easily explained by the mechanics of the system: A stiffer membrane is harder to bend; thus fewer filaments can impinge on it simultaneously. This reduces its effect of load distribution over several filaments and forces concentration on few filaments promotes filament breaking and lamellipodium retractions.

Additional Results. ***Active Layer.*** Fig. 2 *Insets B* (main text) show that branching and capping protection concentrate in a narrow region closely following the membrane during protrusion. In Fig. S3 we give further details on this result from our simulations. Fig. S3 *a* and *b* shows that the branching and the capping protection layers, respectively, follow the membrane more closely when the force is higher. This is easily explained from the fact that smaller overhangs are tolerated when the opposing load is higher, and this leads to more compact structures with free space allowing for polymerization and branching only at the very top of the growing network. The result is confirmed in Fig. S3 *c* and *d*, where the distribution of the actual distance of active barbed ends and active branching sites from the membrane are depicted, respectively. The distributions show that the most of the polymerization and branching activity is concentrated in 2–4 d from the membrane and, again, that the active regions narrow for higher values of forces. The thickness of the active region is slightly larger compared to the estimate in ref. 5 (approximately 1 d), but in this case it arises naturally from the steric hindrance of the filaments and is not governed by biochemical control, which might enhance the concentration in a narrower zone.

Hysteresis. As discussed in the main text, the mechanical organization of the network might explain, at least qualitatively, the hysteretic behavior observed experimentally in ref. 6. In Fig. S4 we show some results on this topic. Fig. S4*a* reports the load history used to test the growth velocity: After 500 growth steps at $1/2F_r$, the force is increased to $5/6F_r$ for 1,000 growth steps and then reduced again to $1/2F_r$ for the following 500 growth steps. The corresponding time history of the velocity is reported in Fig. S4*b* where it is clear that the "training" during the intermediate growth period against a higher load results in a speedup of the lamellipodium in the third period at the same level of force. The result is statistically significant as proved in Fig. S4*c* where we report the velocity distribution computed over 12 independent simulations under the same load history: The velocity distribution shifts toward higher values with an approximately 60% increase in the mean velocity and an approximately 40% increase in the peak of the velocity distribution after the training under larger force.

Preferential Breaking at Branch Junctions. It is well known (7) that phalloidin stabilizes Arp2/3 complexes, which are responsible for the branching of actin filaments. Unstabilized branch junctions might be more fragile and break under smaller forces. To test the effect of branching points stabilization on lamellipodium protrusion we performed simulations with a rupture force of the filaments of 200 pN and rupture force for the branching points of 100 pN. We denote these as "weak junctions" simulations. The Fv diagram for these simulations is almost identical to the one for the benchmark case, as shown in Fig. S5*a*. This shows that lamellipodia protrusion, in our model, is mainly determined by the strength of the weak points in the network. The distribu-

tion of filaments orientation remains symmetric for both sets of parameters but with a wider distribution in the case of weak junctions (compare Fig. S5 *b* and *d*). This might be due to the fact that the increased strength of the filaments allows them to grow longer and bend more. This also induces a qualitative difference in the type of structures arising in organized networks as evident from the comparison of Fig. S5 *c* and *e*: In the benchmark case protrusion relies on the formation of densely branched, V-type structures. In the case of weak junctions, protrusion relies on few long filaments with many short side branches.

Axial Forces on Filaments. In our model polymerization rate does not depend explicitly on the axial force acting on the filaments. However, the filaments on which a monomer is added are not chosen at random, as growth events that would lead to overlaps with preexisting filaments or with the membrane are not allowed (see *Methods*). As a consequence, the axial forces on filaments selected for growth are always rather low. In Fig. S6 we show the cumulated probability distribution of observing an axial force larger than a given value on the filaments eligible for growth according to the criterion described in *Methods*. Axial forces on the tips are computed as the component along the filament axis of the resulting force on the three trusses intercepted by a transverse section on the tip monomer. Compressive forces are assumed to be positive. The distribution is computed on 12 statistically independent histories of growth against different external forces.

1. Kishino A, Yanagida T (1988) Force measurements by micromanipulation of a single actin filament by glass needles. *Nature* 334: 74–76.
2. Tsuda Y, Yasutake H, Ishijima A, and Yanagida T (1996) Torsional rigidity of single actin filaments and actin-actin bond breaking force under torsion measured directly by in vitro micromanipulation. *Proc Natl Acad Sci USA* 93:12937–12942.
3. Arai Y, Yasuda R, Akashi K, Harada Y, Miyata H, Kinosita K, and Itoh H (1999) Tying a molecular knot with optical tweezers. *Nature* 399:446–448.
4. Isambert H, Venier P, Maggs A, Fattoum A, Kassab R, Pantaloni D, and Carlier M (1995) Flexibility of actin filaments derived from thermal fluctuations. Effect of bound nucleotide, phalloidin, and muscle regulatory proteins. *J Biol Chem* 270:11437–11444.
5. Schaus T, Taylor E, Borisy G (2007) Self-organization of actin filament orientation in the dendritic-nucleation/array-treadmilling model. *Proc Natl Acad Sci USA* 104:7086–7091.
6. Parekh S, Chaudhuri O, Theriot J, Fletcher D (2005) Loading history determines the velocity of actin-network growth. *Nat Cell Biol* 7:1219–1223.
7. Nakamura F, Osborn E, Janmey PA, Stossel TP (2002) *J Biol Chem* 277:9148–9154.

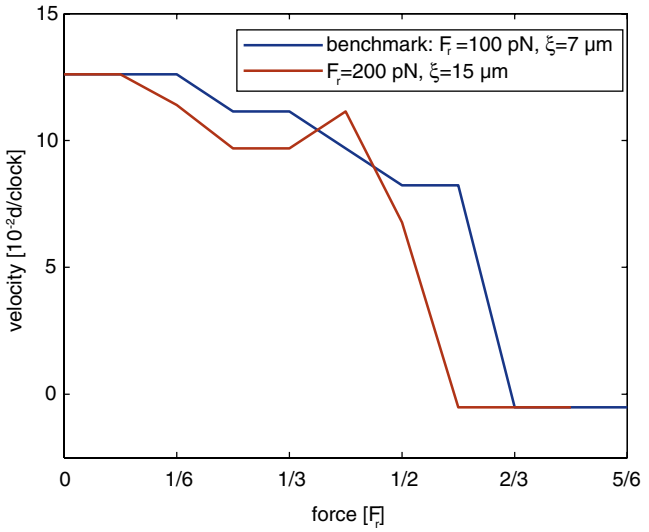

Fig. S1. *Fv* diagrams. Comparison of results obtained with benchmark values of material parameters (see Table S1) with results obtained increasing F_r to 200 pN and ξ to 15 μm.

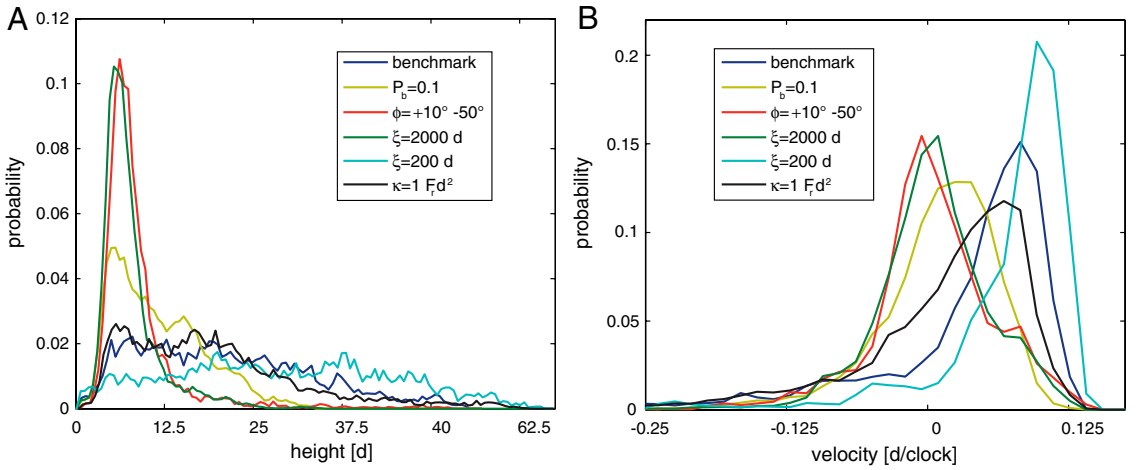

Fig. S2. Parameter sensitivity. Effect of the parameters on the simulations at 30 pN. (*a*) Traces and height distribution and (*b*) mesoscopic velocity histograms.

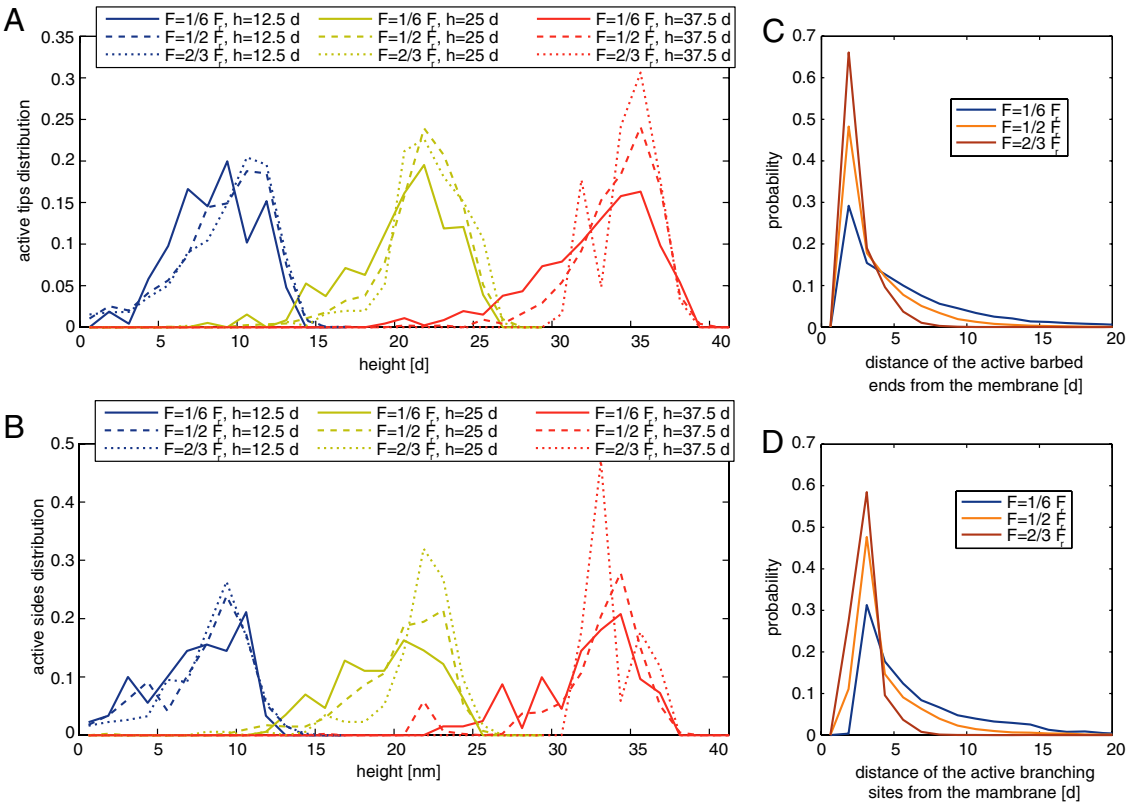

Fig. S3. A narrow branching–capping protection zone arises naturally. (*a*) Distribution of the active barbed ends and (*b*) of the active branching sites over height for different values of the opposing force and mean height of the membrane. (*c*) Distance of the active barbed ends and (*d*) of the active branching sites from the membrane for different values of the force.

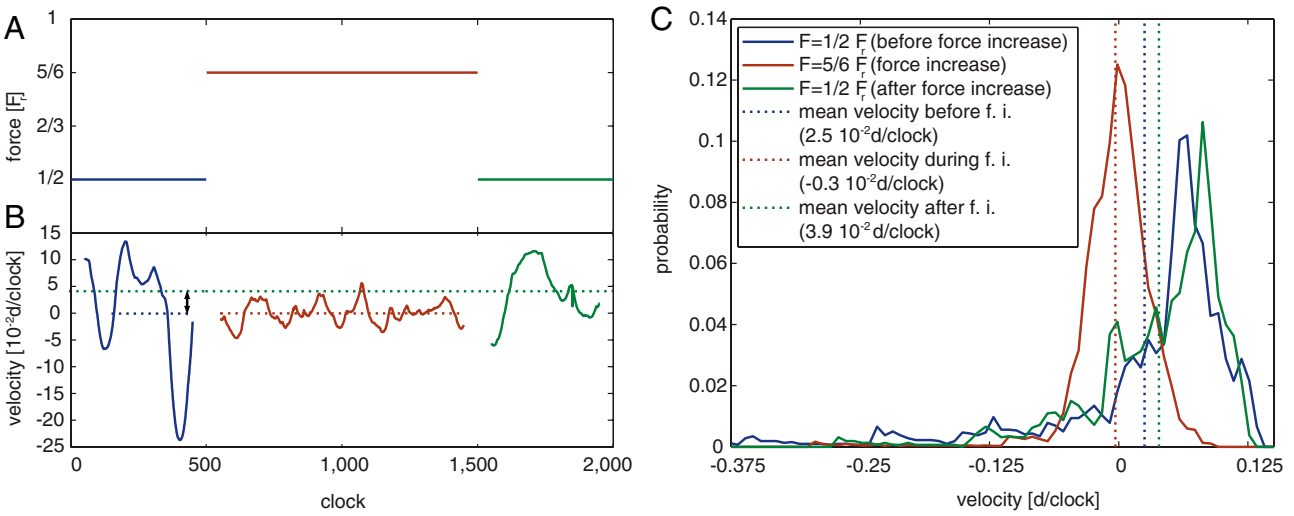

Fig. S4. Dependence on loading history. (*a*) Time history of the force applied to the membrane and (*b*) of the corresponding velocity in a typical simulation. Dotted lines correspond to the mean value of the velocity in each time interval in which the applied force remains constant. (*c*) Velocity distributions and averages for 12 independent simulations with the same history of applied force as in *b*.

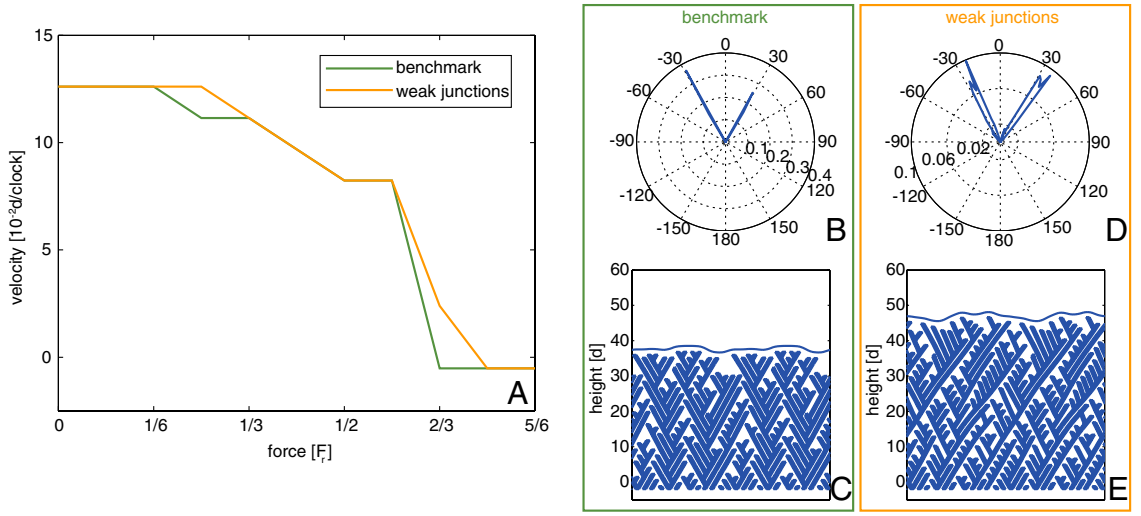

Fig. S5. Weak branch junctions. (*a*) *Fv* diagram for the case of weak junctions compared to the benchmark case. Both diagrams were normalized using the minimum critical force in the network, which is $F_r = 100$ pN for both cases. (*b*) Filament orientation distribution and (*c*) typical configuration for the benchmark simulation. (*d*) Filament orientation distribution and (*e*) typical configuration for the case of weak junctions.

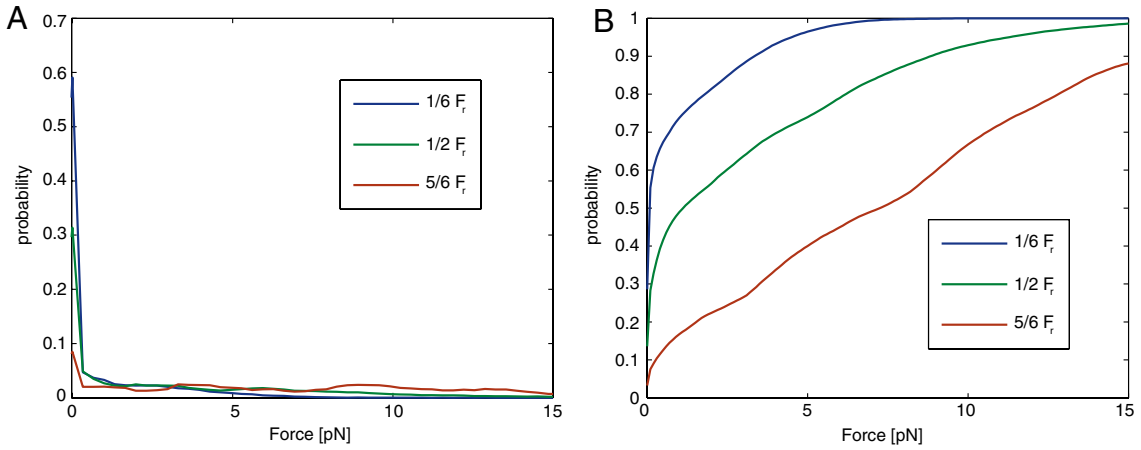

Fig. S6. Axial forces on growing barbed ends. (*a*) Probability histogram and (*b*) cumulate probability distributions of the compressive axial force on barbed ends eligible for growing. Distributions are computed on 12 statistically independent simulations for each force level applied to the membrane.

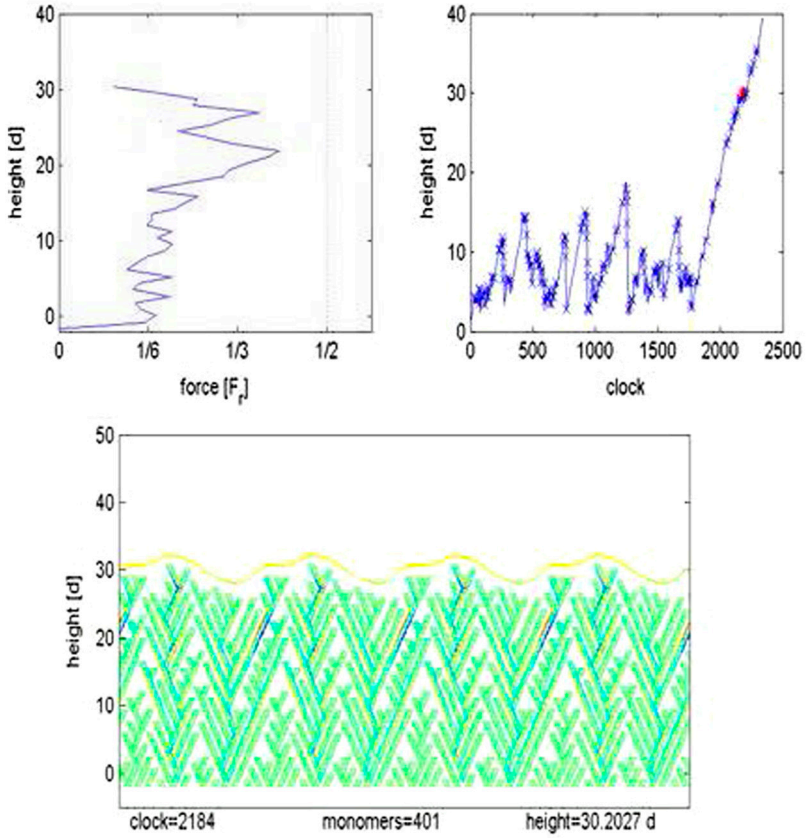

Movie S1. A model actin network growing against a force of 0.5 Fr simulation results using material parameters listed in Table S1.

Movie S1 (MOV)

Table S1. Model parameters

Parameter	Description	Value	Refs.
d	actin filament thickness	7 nm	(1, 2)
β	characteristic angle of the truss structure	60°	
a	monomer edge length	$d\cos(\beta/2)$	
θ	initial orientation of seeds	± 30°	
φ	branching angle	60°	(3–5)
P_b	branching probability	0.3	
D	depolymerization speed	10	
ξ	filament persistence length	$10^3\ d$	(6, 7)
F_r	filament rupture force	100 pN	(8)
f_c	edge rupture force	$F_r/2$	
E_m	membrane stretching stiffness	$2F_r$	(9, 10)
κ	membrane bending stiffness	$0.1F_r \cdot d^2$	(5)
c	contact stiffness	30 pN · nm	
δ	contact length	$0.5a$	

Parameters for the benchmark simulations in units of filament thickness d and filament rupture force F_r.

1. Alberts B, Johnson A, Lewis J, Raff M, Roberts K, Walter P (2008) *Molecular Biology of the Cell* (Garland Science, New York).
2. Pollard TD, Earnshaw WC (2008) *Cell Biology* (Saunders, New York).
3. Schaus T, Taylor E, Borisy G (2007) Self-organization of actin filament orientation in the dendritic-nucleation/array-treadmilling model. *Proc Natl Acad Sci USA* 104:7086–7091.
4. Carlsson AE (2003) Growth velocities of branched actin networks. *Biophys J* 84:2907–2918.
5. Atilgan E, Wirtz D, Sun S (2005) Morphology of the lamellipodium and organization of actin filaments at the leading edge of crawling cells. *Biophys J* 89:3589–3602.
6. Isambert H, Venier P, Maggs A, Fattoum A, Kassab R, Pantaloni D, and Carlier M (1995) Flexibility of actin filaments derived from thermal fluctuations. Effect of bound nucleotide, phalloidin, and muscle regulatory proteins. *J Biol Chem* 270:11437–11444.
7. Gittes F, Mickey B, Nettleton J, Howard J (1993) Flexural rigidity of microtubules and actin filaments measured from thermal fluctuations in shape. *J Cell Biol* 120:923–934.
8. Kishino A, Yanagida T (1988) Force measurements by micromanipulation of a single actin filament by glass needles. *Nature* 334: 74–76.
9. Wolfe J, Steponkus P (1983) Mechanical properties of the plasma membrane of isolated plant protoplasts: Mechanism of hyperosmotic and extracellular freezing injury. *Plant Physiol* 71:276–285.
10. Morris C, Homann U (2001) Cell surface area regulation and membrane tension. *J Membr Biol* 179:79–102.